A Dusty Atmospheric River Brings Floods to the Middle East

Amin Dezfuli[1,2,*], Michael G. Bosilovich[1], and Donifan Barahona[1]

[1]*Global Modeling and Assimilation Office, NASA Goddard Space Flight Center, Greenbelt, MD, USA*
[2]*Science Systems and Applications, Inc., Lanham, MD, USA*
**Corresponding author (amin.dezfuli@nasa.gov)*

Key Points:

- Atmospheric rivers can cause heavy rains, rapid snowmelt, and floods in regions far from the oceans such as the Middle East.
- A distinct characteristic of ARs in the Middle East is their contribution to dust transport from the major sources along their pathways.
- Based on its intensity and duration, the AR in this study is classified as "balance of beneficial and hazardous".

Abstract

Torrential rainfall and rapid snowmelt in April 2017 caused deadly floods in northwestern Iran. An atmospheric river (AR), propagating across the Middle East and North Africa, was found responsible for this extreme event. The snowmelt was triggered by precipitation and warm advection associated with the AR. Total satellite-based rainfall for April 2017 was moderately below normal, suggesting that a heavy flood can happen during dry years. The AR was fed by moisture from the Mediterranean and Red Seas. Despite its adverse societal consequences, this event was beneficial to the recovery of the desiccating Lake Urmia. The impacts of this AR were not limited to flooding; it also facilitated dust transport to the region. This distinct characteristic of the ARs in the Middle East is attributed to major mineral dust sources located along their pathways. This event was reasonably predicted at 7-day lead time, crucially important for successful early warning systems.

Plain Language Summary

The frequency and intensity of weather-related extreme events, particularly floods, have increased in recent decades, both globally and in parts of the Middle East. Some floods are caused by heavy rains from the atmospheric rivers (AR), which are long, narrow, and transient corridors of strong horizontal water vapor transport. The contribution of ARs to precipitation extreme events over the Middle East is not well understood. Here, we show that a 2017 devastating flood in northwestern Iran that claimed 48 lives was driven by a ~5,500 km long AR, which extended from northeastern Africa to Central Asia. The impacts of this event were not limited to heavy floods; strong winds within the AR also carried mineral dust from the sources located on their pathway to the region. From a different perspective, the rains were much needed for restoration of the desiccating Lake Urmia in northwestern Iran. Numerical weather predictions provided a skillful forecast for this multi-impact event at up to a 7-day lead time. This is important because such events have various societal, health and environmental implications, and their skillful predictions would be beneficial for decision makers.

1. Introduction

The frequency and intensity of extreme weather-related hazards, particularly floods, have increased in recent decades, both globally and in parts of the Middle East (Banholzer et al. 2014; Modarres et al. 2016; Razavi et al. 2020). The regions with poor infrastructures and dry climate, such as many parts of the Middle East, have been in particular vulnerable to the impacts of these events (Zereini and Hötzl 2008; Masih et al. 2011; Gleick 2014; Rougé et al. 2018; Hameed et al. 2019). The countries in the region have experienced a range of environmental issues such as widespread floods, prolonged droughts, dust storms, heat waves, and desiccating lakes (e.g., Zhang et al. 2005; Raziei et al. 2009; Furman 2003; Lelieveld et al. 2016; Dezfuli et al. 2017; Alborzi et al. 2018). These extreme events result from interactions between several atmospheric features that act across spatio-temporal scales (Figure 1). Understanding these processes, especially those associated with two or more concurrent natural hazards, i.e., compound events, is crucial for disaster management.

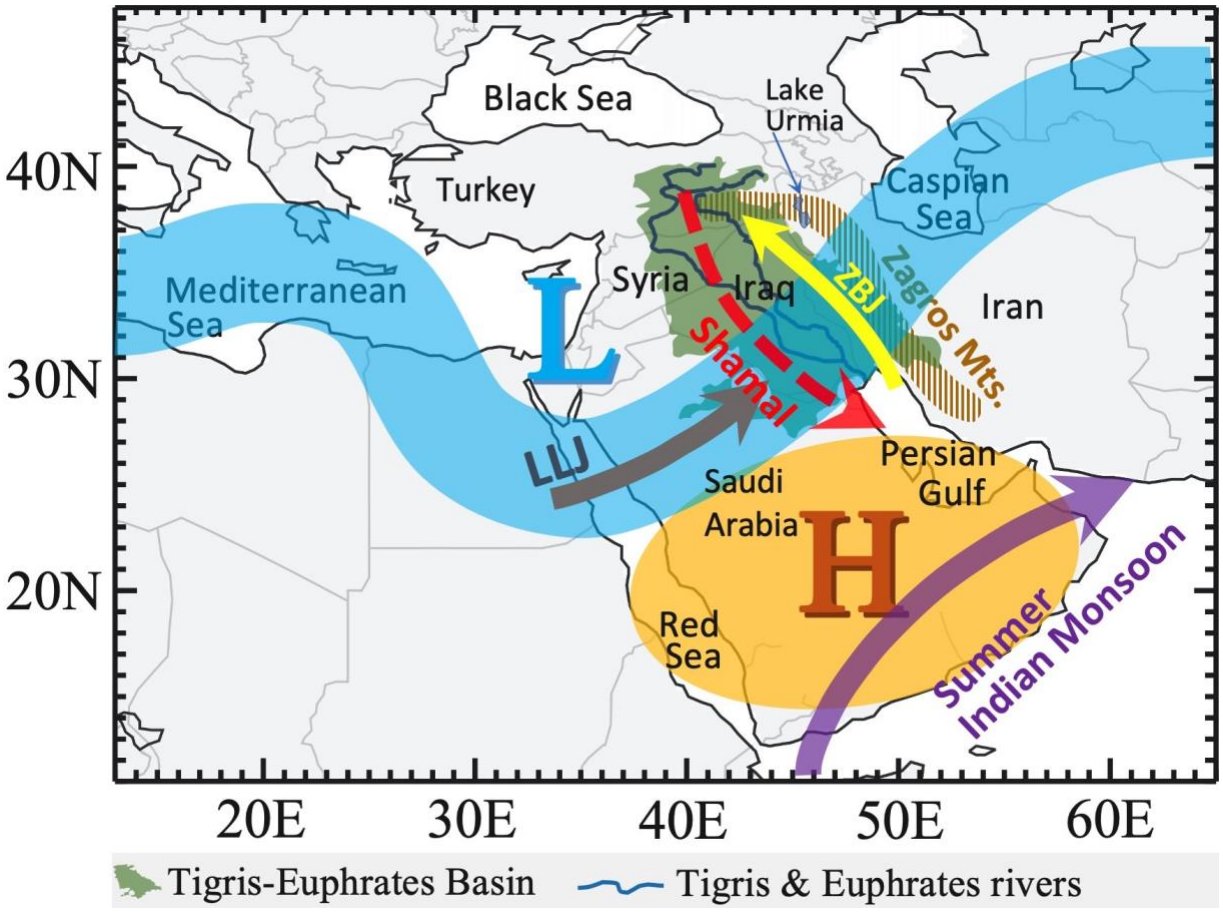

Figure 1. *Regional drivers of weather and climate over the Middle East, adapted from Dezfuli et al. (2017) with modification (© American Meteorological Society, used with permission). The phenomena schematically shown include a typical mid-latitude storm, low-level jet (LLJ), summer Indian monsoon, Zagros barrier jet (ZBJ), Shamal winds and several geographical features such as the Zagros Mountains and the regional seas.*

Some of the heavy rains and associated floods around the globe are attributed to the atmospheric rivers (AR). An AR is defined as "*a long, narrow, and transient corridor of strong horizontal water vapor transport that is typically associated with a low-level jet stream ahead of the cold front of an extratropical cyclone*" (Ralph et al. 2018). The impacts of ARs on coastal regions like the western U.S. and Europe have been extensively studied (e.g., Ralph et al. 2006; Lavers and Villarini 2015; Ramos et

al. 2016; Collow et al. 2020). However, their role in extreme precipitation and rapid snowmelt leading to heavy floods over the Middle East has only recently received attention (de Vries et al. 2013; Tubi et al. 2017; Akbary et al. 2019; Dezfuli 2020; Esfandiari et al. 2020; Massoud et al. 2020; Bozkurt et al. 2021). That limited body of research has attempted to shed light on the mechanisms of the ARs or statistical characteristics of their future changes. These studies suggest that the ARs in the region, which are associated with rainfall, primarily impact Iran due to orographic effects of the Zagros Mountains. The Red and Mediterranean Seas and Atlantic Ocean serve as the main moisture sources for these ARs.

Like other hydro-meteorological extremes, accurate forecast of ARs is crucial for decision makers. However, deterministic forecast of this weather phenomenon is also limited to ~7-day lead time due to the chaotic nature of the atmosphere (Baggett et al. 2017; Cordeira et al. 2017; Martin et al. 2018). We also speculate that the degree of prediction skill might be partly related to the sparse regional observational network. The forecast error in landfall location of ARs, for example, at 5-day lead can exceed 500 km (Wick et al. 2013). Some efforts have been made to extend the forecast lead times using probabilistic approaches and incorporating climate modes of variability such as the Madden-Julian oscillation (Mundhenk et al. 2018; DeFlorio et al. 2019).

Here, we examine the role of an atmospheric river in the floods of April 14, 2017 in northwestern Iran. That event claimed 48 lives, one of the deadliest in the past several decades in the region (Presstv 2017). The casualties happened primarily in rural areas by flash floods and partly due to the lack of effective early warning systems. However, from a different perspective, heavy rains in northwestern Iran may be much needed as they would facilitate recovery of the desiccating Lake Urmia. This saline lake has shrunk sharply between 1996 and 2016 (Alborzi et al. 2018; Danesh-Yazdi and Ataie-Ashtiani 2019) and some of its dried parts have emerged into potential dust sources, resulting in health and environmental consequences (Boroughani et al. 2019).

Given its various implications discussed above, this extreme event would provide an opportunity to shed light on the mechanisms and impacts of the ARs in the region. As such, the purpose of this analysis is three-fold. First, due to the lack of research on atmospheric rivers in the region, we present a general overview of the characteristics of this AR. That includes its horizontal structure, the precipitation amount resulted from the AR and how it compares to the regional climatology, and the AR pattern in the context of a mid-latitude synoptic system. Second, we investigate specific characteristics that reflect regional natural features. That includes the contribution of regional moisture sources to the AR and the possibility of enhanced dust transport within the AR corridor. Third, the skill of short-to medium-range numerical prediction of this AR is evaluated since better forecast of similar events would improve early warning systems and help mitigating their adverse impacts.

2. Data

Various NASA products are used for diagnostics and predictions. They include daily and monthly precipitation data from the Integrated Multi-satellitE Retrievals for GPM (IMERG) Version 06 (Huffman et al. 2015). The data is available at 0.1° horizontal resolution from June 2000 to near real time. We were not able to find publicly available ground-based observations for precipitation to use in our analysis. Daily meteorological data (specific humidity, horizontal winds, potential temperature, and 2-meter temperature) and dust column mass density are obtained from the Modern-Era Retrospective Analysis for Research and Applications, version 2 (MERRA-2, Gelaro et al. 2017). The data is available at 0.5° × 0.625° regular latitude by longitude grids and assimilates aerosol optical depth (AOD). All data sets can be accessed from https://disc.gsfc.nasa.gov. The AR is identified by

analyzing vertically integrated water vapor transport (IVT) over the 1000-300 hPa layer from MERRA-2 data. The Visible Infrared Imaging Radiometer Suite (VIIRS) Corrected Reflectance imagery is used to detect thick ice and snow. The VIIRS instrument is on board the joint NASA/NOAA Suomi National Polar orbiting Partnership (Suomi NPP) satellite (Román et al. 2018). The VIIRS Corrected Reflectance for days before and after the event were obtained from NASA Worldview Mapping Application (https://worldview.earthdata.nasa.gov).

The weather forecasts were produced with version 5.16 of the Goddard Earth Observing System (GEOS), used at the time of the event. That version underwent several updates, compared to version 5.12.4 that was used in MERRA-2. The major changes include a transition from a three-dimensional to a four-dimensional assimilation system, a four-fold (linear) increase in spatial resolution to a 12.5-km, and improvement in the representation of atmospheric processes in the GEOS model (Molod et al. 2015). These changes led to more realistic features in the assimilated fields and better quality of the medium-range forecasts. The forecasts are available at 0.25° × 0.3125° regular latitude by longitude grids. For consistency, the Reanalysis from this version of the model is used to evaluate the IVT forecasts.

3. Causes of the heavy rains

Torrential rainfall on April 14, 2017 caused heavy flooding and landslides over northwestern Iran. The areal average of the satellite-based rainfall was 15.6 mm, approximately equivalent to the 99th percentile of the April daily rainfall over the 2001-2020 period (Figure 2a). A maximum value of ~48 mm was reported in some stations located near the city of Tabriz (IRNA 2017). However, the time-series of monthly total satellite-based precipitation shows that April 2017 was a relatively dry month (Figure 2b). This is intriguing because it shows that an extreme rainfall event can happen in fact during an anomalously dry season.

Analysis of IVT reveals that an atmospheric river was responsible for the heavy rains (Figure 2c). The horizontal pattern of the AR was captured using a 250 kg m^{-1} s^{-1} IVT threshold. The ~5,500 km long AR extended from northeastern Africa across the Middle East as it reached Central Asia. At its northeastern edge, the AR poured rainfall over another drying inland water body, the Aral Sea, which has shrunk to 10% of its original size since 1960 (Micklin 2010; Wurtsbaugh et al. 2017). Maximum precipitation occurred over the Lake Urmia Basin and extended to parts of Turkey and Iraq, consistent with orographic forcing associated with the AR passing over the Zagros Mountains. The daily regional mean IVT in April was overall larger during the three wettest years than the three driest years. However, the IVT associated with the event presented here had the largest value over 2001-2020 (Figure S1).

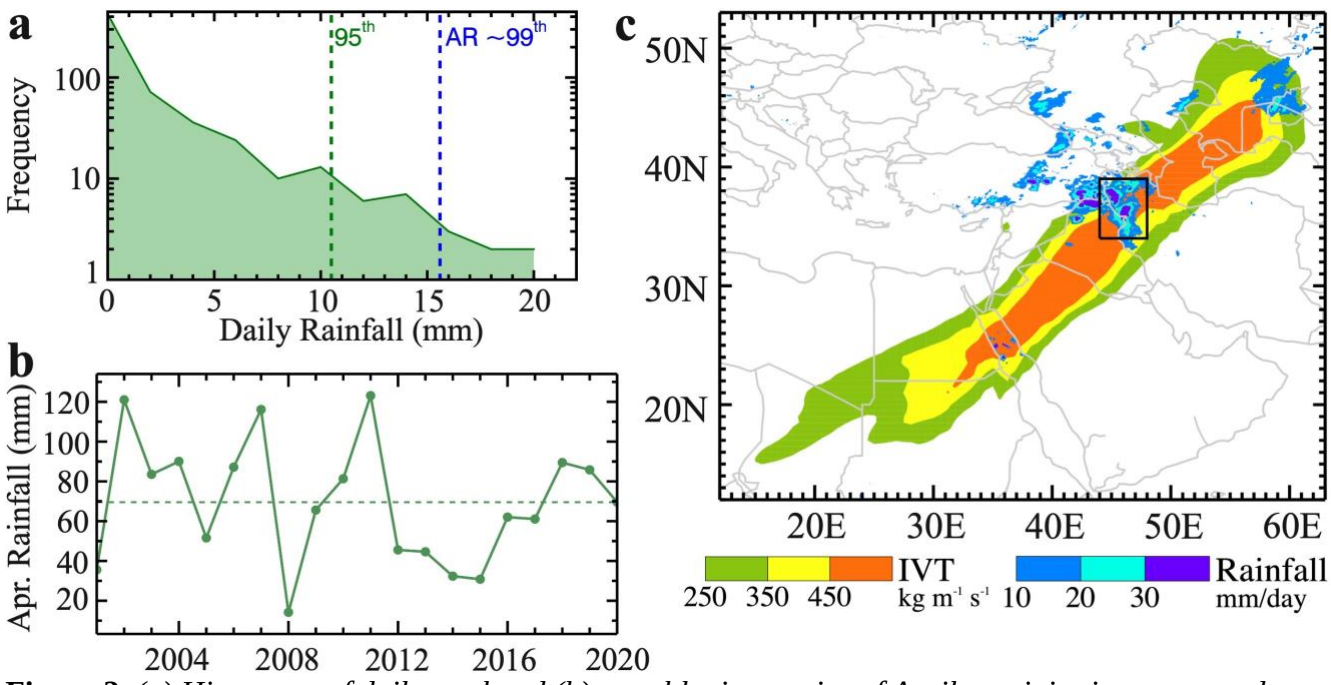

Figure 2. *(a) Histogram of daily total and (b) monthly time-series of April precipitation, averaged over northwestern Iran (black box in (c)). Blue dashed line represents the rainfall over April 14, 2017. (c) Horizontal patterns of the vertically integrated water vapor transport (IVT) and rainfall during April 14, 2017. Precipitation data in all panels is from the satellite-based IMERG product.*

4. Dust transport within the AR

ARs are generally associated with strong horizontal winds in the lower troposphere (Waliser and Guan 2017; Voss et al. 2020). The ARs affecting our study region often travel through some of the world's major sources of mineral dust located in deserts of the Middle East and North Africa (Boloorani et al. 2014; Cao et al. 2015; Nabavi et al. 2016). This unique regional characteristic motivated us to examine whether this AR was associated with dust transport, as recently shown by Chakraborty et al. (2021). We compared dust column mass density during April 14, 2017 with its long-term mean and found a positive anomaly within the AR corridor (Figure 3). About 80% of the AR area has a z-score of greater than +1.28 (>90th percentile), and the average z-score within the AR is +2.18 (>98th percentile).

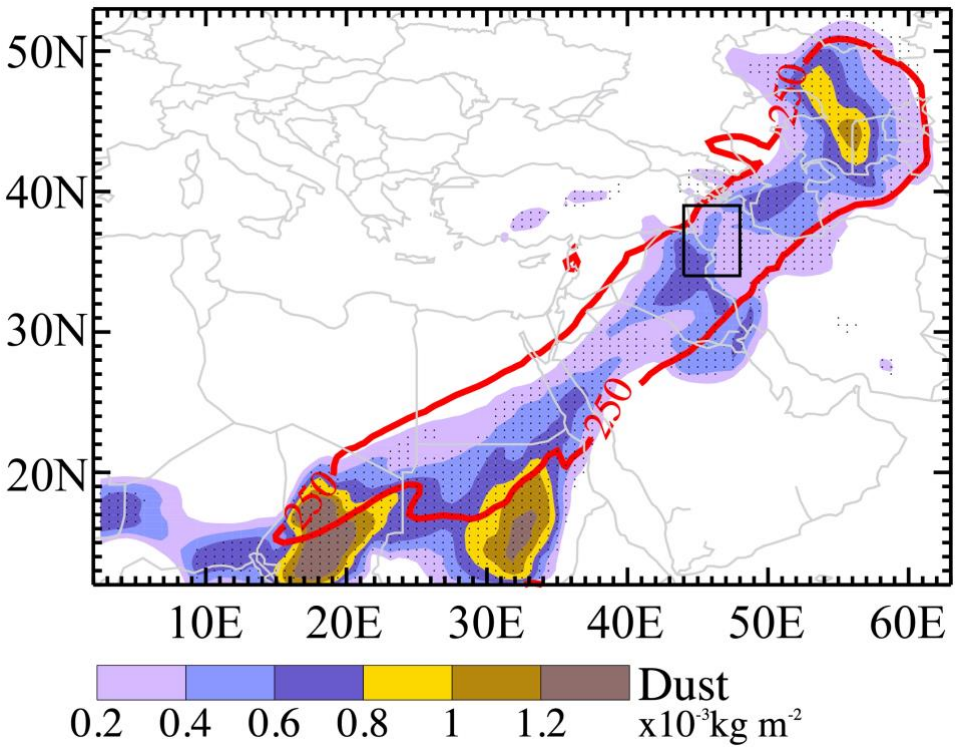

Figure 3. *Dust column mass density during April 14, 2017 minus its long-term mean (1981-2020, excluding 2017) over a one-week window around that day (i.e., April 11-17). Thick red line shows the AR extent detected by an IVT value of 250 kg m^{-1} s^{-1}. Dotted area is where z-score is greater than +1.28 (>90th percentile).*

5. Synoptic diagnostics of the AR

ARs are typically located along cold fronts associated with mid-latitude cyclones (Ralph et al. 2004; Dacre et al. 2015). Analysis of potential temperature at 700 hPa during this event identified a cold front coincident with the AR (Figure 4a). The low-level jet ahead of the front also appeared over the same region, contributing to water vapor transport along the AR. Vertical cross-sections of moisture flux towards the AR corridor showed that the Mediterranean and Red Seas both supplied moisture from the levels below 850 hPa (Figure 4b,c). The Red Sea seems to have a more intense but horizontally narrower moisture flux than the Mediterranean. The moisture contribution of these two seas on April 13 (Figure S2) was generally similar to the patterns observed during the event. This AR started to develop on April 13, reached its maximum intensity on April 14 as approached northwestern Iran, and propagated southeastward in the next three days as it gradually dissipated (Figure S3).

As the water vapor from these two sources flows toward the AR and the cold front advances, the moisture flux converges and is swept up. This dynamical forcing combined with the topographically-driven uplift over land led to vertical expansion of the moisture flux (Figure 4d). However, its maximum value remains below 700 hPa level before the AR approaches the Zagros Mountains, where the moisture laden air condenses as it flows upslope, resulting in the extreme precipitation event. The heavy rains reinforced by rapid snowmelt from the highlands located to the east of Lake Urmia caused the floods (Figure 4e,f). Satellite images taken before and after the event show a reduction of nearly half the snow surface. This reduction may be attributed to both rainfall and warm advection associated with the AR. As the AR approached the region (Figure S3), the 2-meter air temperature increased by ~8 K in hours preceding the rainfall event (Figure 4g). The characteristics of this AR, including its interaction with mountains, are quite similar to the ARs analyzed in Bozkurt et al. (2021).

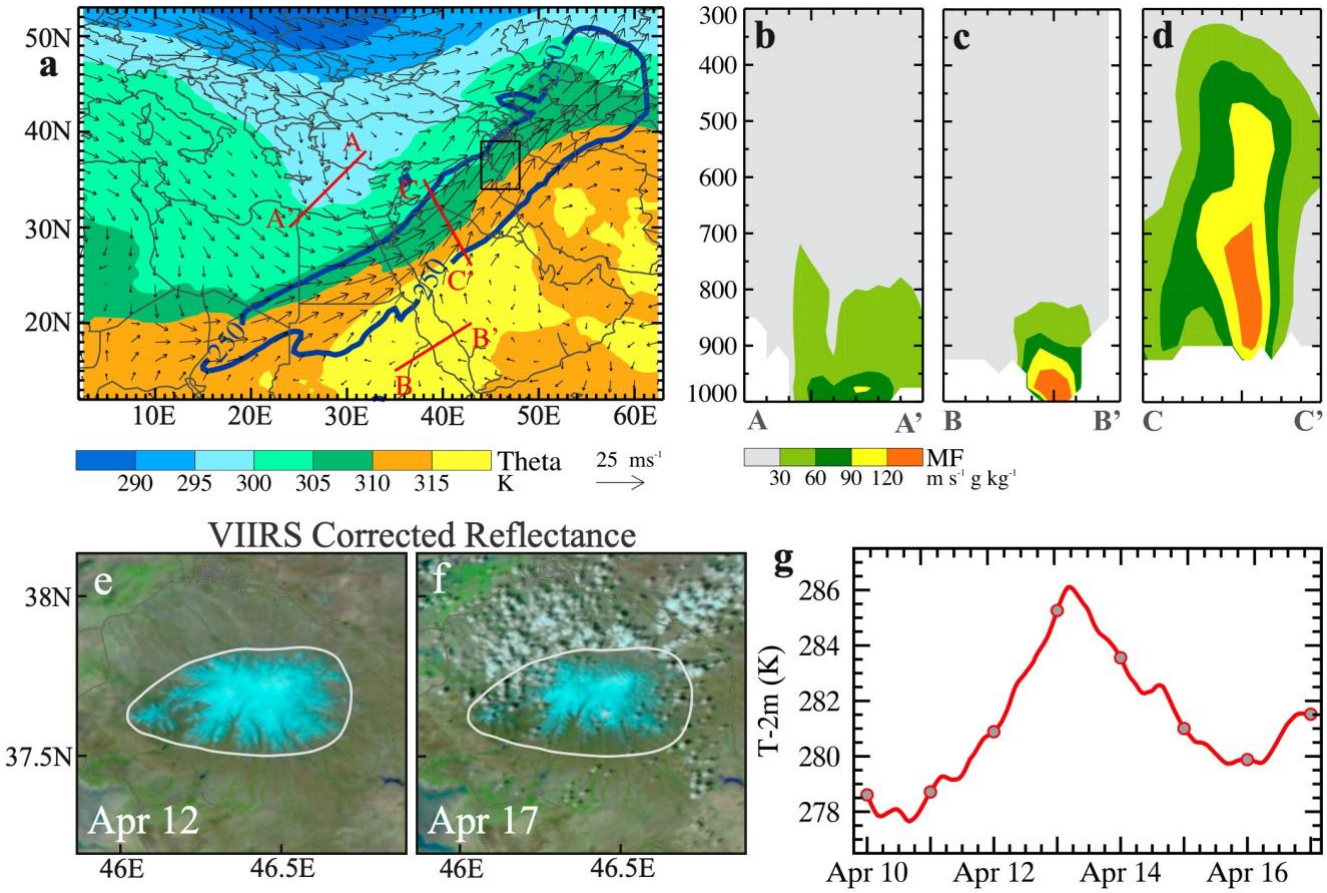

Figure 4. *(a) Potential temperature (shading) and horizontal winds (arrows) at 700 hPa on April 14, 2017. The thick dark blue line shows the AR extent detected by an IVT value of 250 kg m^{-1} s^{-1}. (b-d) Vertical cross-sections of moisture flux (MF) across A-A' (Mediterranean Sea), B-B' (Red Sea) and C-C', respectively. Positive values represent the flux perpendicular to the vertical plane towards the AR corridor. (e-f) VIIRS corrected reflectance for days prior and after the event obtained from NASA Worldview. Areas of thick ice and snow are shown in vivid sky blue. Note that the region plotted in (e) and (f) is located within the black box shown in (a). (g) The 24-hour running average of hourly 2-meter temperature, averaged over the region shown in (e) and (f) for the days prior, during, and after the event.*

6. Predictability of the event

Here, we have evaluated the performance of deterministic forecasts provided by NASA's GEOS model at lead times of 1, 3, 5, and 7 days. To allow comparison with reanalysis and satellite-based observations, the same variables as those shown in Figure 2c, i.e., rainfall and IVT, are used (Figure 5a-d). However, for consistency the IVT is compared with the Reanalysis from the same GEOS model version that was used for forecasts (Figure S4). A qualitative assessment of the IVT patterns shows that the AR structure is reasonably captured up to a 5-day lead, before its horizontal extent starts to shrink, and its axis retracts ~150 km southeastward compared to Reanalysis from the GEOS model. In order to quantify the prediction skills, we have evaluated the regional mean precipitation, which is the main concern for impact analysis (Figure 5e). The 1-day lead forecast is nearly the same as the satellite-based observations. The forecasts at 3 and 5-day leads show an approximately 20% overestimation, which is within an acceptable range given the uncertainties from IMERG observations. The overestimation grows with lead time and reaches 43% at 7-day lead. However, the IVT forecast

decreases at longer lead-times, although the range of its percent difference is much narrower than that of precipitation.

The precipitation forecasts appear to be predominantly controlled by the "large-scale" processes in the GEOS model as opposed to its convective parameterization. The "large-scale" precipitation component is generated by stratiform clouds that form when the grid-scale humidity is near saturation (Bacmeister et al. 2006). Therefore, how the model resolves dynamical properties such as moisture flux convergence would determine the magnitude of precipitation forecasts at different lead-times.

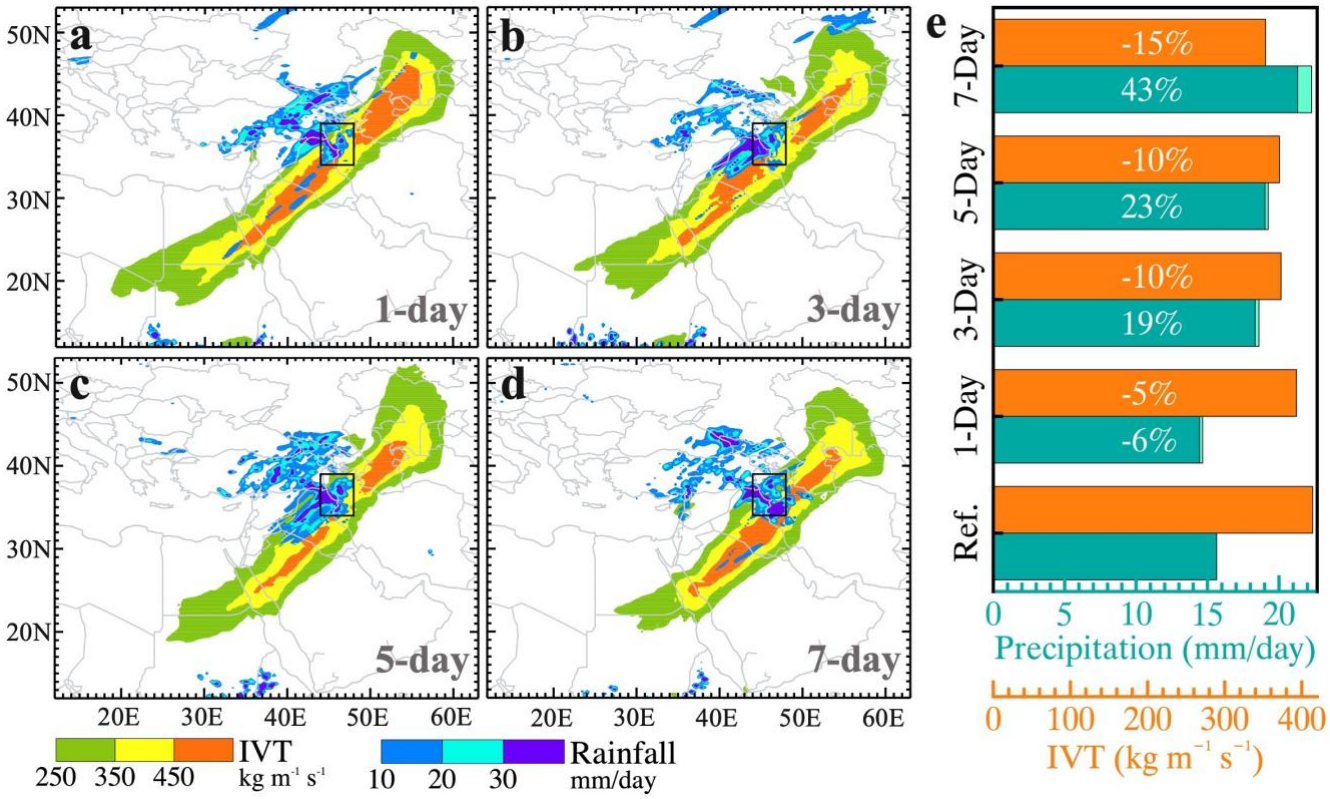

Figure 5. *(a-d) Forecasts of IVT and rainfall for April 14, 2017 provided by NASA's GEOS model at lead times of 1, 3, 5, and 7 days, respectively. (e) Comparing regional mean rainfall (dark green bars) and IVT (orange bars) from the GEOS model forecasts at different lead times with reference data (the lowest bars). The reference data are satellite-based IMERG precipitation and the GEOS model Reanalysis, respectively. For consistency, the Reanalysis is obtained from the same version of the model used for forecasts. Both "large-scale" (dark green) and "convective" (light green) components of precipitation forecast are presented. The white number on each bar shows the percent difference between forecast and its corresponding reference data.*

7. Discussion and conclusions

High-impact weather events, particularly those with multiple consequences that occur in vulnerable regions like the Middle East, have significant socio-environmental implications. The atmospheric river presented here is one such event. Understanding the mechanisms of similar events, their impacts and potential predictability would be valuable for decision-makers.

A simple framework is laid out to tie both physical and decision-making aspects of the AR-related research and place the current analysis into a broader context (Figure 6). Several future directions along with their interconnections are identified. One area of research would involve improvement in

prediction skills, for example, through development of hybrid dynamical-statistical approaches. Better predictions would help designing more effective early warning systems and disaster management strategies, which would result in mitigating the impacts of such extreme events. Another research aspect may focus on analyzing the future AR characteristics in climate projections from the coupled model intercomparison project phase 6 (CMIP6). This effort would allow us to investigate the potential future changes in ARs over the region and incorporate that information into long-term planning for water resources and disaster management.

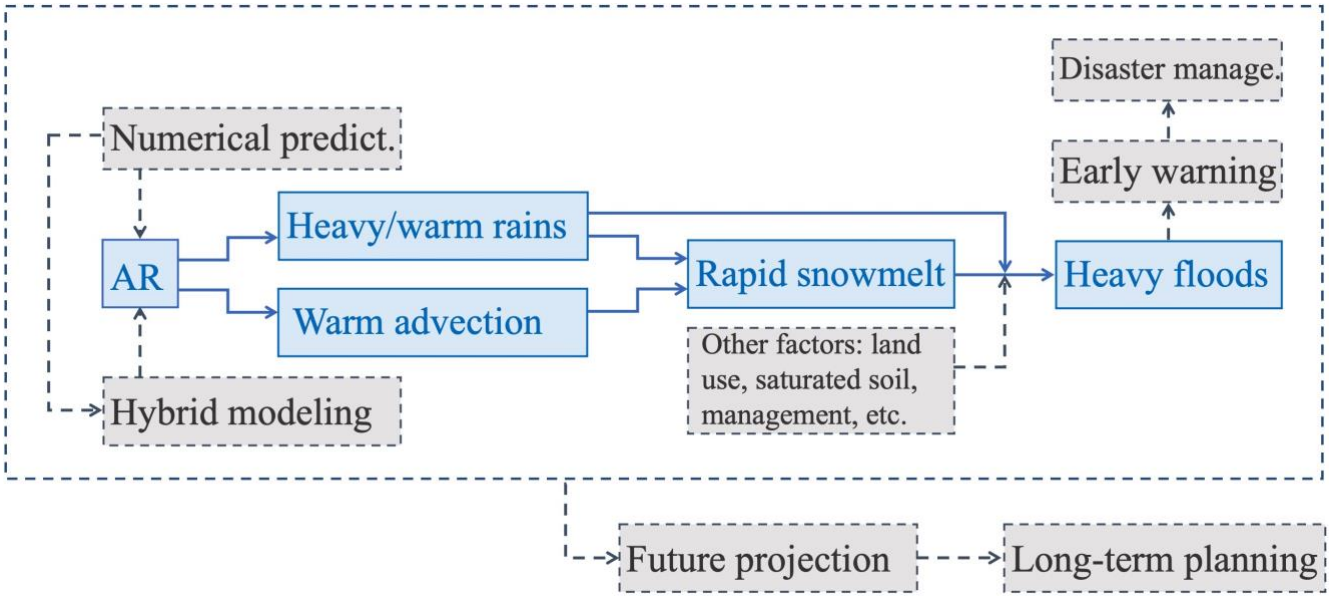

Figure 6. *A framework proposed to incorporate atmospheric rivers into short to long-term planning. Blue boxes show aspects of the AR analysis addressed in the current study. Gray boxes put the current analysis into a broader context, highlighting potential future directions on improvement of predictions, early warning systems, and long-term projection of ARs.*

Although other parts of the country were also affected, this study has focused on the first day of the event when the maximum impacts occurred over the Lake Urmia Basin. Using a recently developed scale that characterizes ARs based on their intensity and impacts (Ralph et al. 2019), this AR would be classified as Category 3. That is because maximum instantaneous IVT at given locations within northwestern Iran exceeded 1,000 kg m^{-1} s^{-1} and maintained AR conditions (i.e., IVT ≥ 250 kg m^{-1} s^{-1}) for 24 hours coincident with the event. This category represents "*balance of beneficial and hazardous*", which is broadly consistent with the nature of this event that adversely affected the people due to its heavy floods but positively contributed to restoration of the drying Lake Urmia.

Despite some recent efforts, mechanisms and impacts of ARs in the Middle East remain relatively understudied. This work, as a follow up to a recent related case study (Dezfuli 2020), aims to improve our understanding of the AR characteristics over the region. Unlike the first study that found an AR responsible for the record floods during an anomalously wet year, current analysis shows that the 2017 event occurred in a relatively dry year. This contrast suggests that individual extreme precipitation events can happen in seasons with both above and below normal conditions. However, further analysis is needed to create a climatology of ARs in the region that would facilitate comparison of their frequency during dry and wet years. Using a percentile-based threshold for IVT may be a more practical approach to detect the AR events in drier regions like the Middle East. For example, the global AR catalogue compiled by Guan and Waliser (2015; 2019) was able to identify the atmospheric

river presented in the current study. Another finding in our analysis was the important contribution of ARs to rapid snowmelt over the Zagros Mountains, consistent with the recent work by Bozkurt et al. (2021).

In addition, this study reveals some characteristics specific to the ARs in the Middle East, differentiating them from those observed along the well-studied coastal regions of North America and Europe. As shown here, one difference pertains to dust transport facilitated by major mineral dust sources within the ARs corridor in the region. This is important because dust storms have been associated with serious health issues over the Middle East (Khaniabadi et al. 2017; Soleimani et al. 2020). In the current study, it seems that both AR and the dust anomaly within its passage are associated with the same underlying dynamics. Also, from the earth system modeling perspective, we speculate that dust aerosols carried by this AR might have affected the precipitation through microphysical processes (Ralph et al. 2016; Voss et al. 2020). Better understanding of such feedback mechanisms is a part of our ongoing research that could offer further improvements in prediction skills and therefore help mitigating the adverse impacts of weather-related extreme events. Another difference is related to the contribution of regional waters, such as the Mediterranean and Red Seas, to AR's moisture content. However, overall synoptic-scale weather patterns of this AR are quite typical. Also worth noting is that our study region and the western U.S. bear several geographical similarities, including presence of a southeast–northwest-oriented mountain range that contributes to precipitation formation (Dezfuli 2020).

8. Acknowledgments

This study was supported by the Global Modeling and Assimilation Office (GMAO) Core funding, provided under NASA's Modeling, Analysis and Prediction (MAP) program. The authors would like to appreciate constructive discussions with members of the National Climate Assessment (NCA) group at GMAO, particularly Allison Collow, as well as inputs and supports from Andrea Molod, Nathan Arnold and Robert Lucchesi of GMAO and Martin Ralph of UCSD. Also, comments from the two reviewers were very valuable. All data used in this study are provided by NASA Goddard Space Flight Center and are publicly available from the following links: winds and temperature at pressure levels (10.5067/QBZ6MG944HW0), T-2m (10.5067/9SC1VNTWGWV3), dust (10.5067/KLICLTZ8EM9D), daily IMERG (10.5067/GPM/IMERGDF/DAY/06), monthly IMERG (10.5067/GPM/IMERG/3B-MONTH/06), and VIIRS corrected reflectance (http://dx.doi.org/10.5067/VIIRS/VNP09GA_NRT.001).

References:

Akbary, M., Salimi, S., Hosseini, S.A. and Hosseini, M., 2019. Spatio-temporal changes of atmospheric rivers in the Middle East and North Africa region. *International Journal of Climatology*, *39*(10), pp.3976-3986.

Alborzi, A., Mirchi, A., Moftakhari, H., Mallakpour, I., Alian, S., Nazemi, A., Hassanzadeh, E., Mazdiyasni, O., Ashraf, S., Madani, K. and Norouzi, H., 2018. Climate-informed environmental inflows to revive a drying lake facing meteorological and anthropogenic droughts. *Environmental Research Letters*, *13*(8), p.084010.

Bacmeister, J.T., Suarez, M.J. and Robertson, F.R., 2006. Rain reevaporation, boundary layer–convection interactions, and Pacific rainfall patterns in an AGCM. *Journal of the Atmospheric Sciences*, *63*(12), pp.3383-3403.

Baggett, C.F., Barnes, E.A., Maloney, E.D. and Mundhenk, B.D., 2017. Advancing atmospheric river forecasts into subseasonal-to-seasonal time scales. *Geophysical Research Letters*, *44*(14), pp.7528-7536.

Banholzer, S., Kossin, J. and Donner, S., 2014. The impact of climate change on natural disasters. In *Reducing disaster: Early warning systems for climate change* (pp. 21-49). Springer, Dordrecht.

Boloorani, A.D., Nabavi, S.O., Bahrami, H.A., Mirzapour, F., Kavosi, M., Abasi, E. and Azizi, R., 2014. Investigation of dust storms entering Western Iran using remotely sensed data and synoptic analysis. *Journal of Environmental Health Science and Engineering*, *12*(1), pp.1-12.

Boroughani, M., Hashemi, H., Hosseini, S.H., Pourhashemi, S. and Berndtsson, R., 2019. Desiccating Lake Urmia: a new dust source of regional importance. *IEEE Geoscience and Remote Sensing Letters*, *17*(9), pp.1483-1487.

Bozkurt, D., Sen, O.L., Ezber, Y., Guan, B., Viale, M. and Caglar, F., 2021. Influence of African Atmospheric Rivers on Precipitation and Snowmelt in the Near East's Highlands. *Journal of Geophysical Research: Atmospheres*, 126, e2020JD033646.

Cao, H., Amiraslani, F., Liu, J. and Zhou, N., 2015. Identification of dust storm source areas in West Asia using multiple environmental datasets. *Science of the Total Environment*, *502*, pp.224-235.

Chakraborty, S., Guan, B., Waliser, D.E., da Silva, A.M., Uluatam, S. and Hess, P., 2021. Extending the Atmospheric River Concept to Aerosols: Climate and Air Quality Impacts. *Geophysical Research Letters*, *48*(9), p.e2020GL091827.

Collow, A.B.M., Mersiovsky, H. and Bosilovich, M.G., 2020. Large-Scale Influences on Atmospheric River–Induced Extreme Precipitation Events along the Coast of Washington State. *Journal of Hydrometeorology*, *21*(9), pp.2139-2156.

Cordeira, J.M., Ralph, F.M., Martin, A., Gaggini, N., Spackman, J.R., Neiman, P.J., Rutz, J.J. and Pierce, R., 2017. Forecasting atmospheric rivers during CalWater 2015. *Bulletin of the American Meteorological Society*, *98*(3), pp.449-459.

Dacre, H.F., Clark, P.A., Martinez-Alvarado, O., Stringer, M.A. and Lavers, D.A., 2015. How do atmospheric rivers form?. *Bulletin of the American Meteorological Society*, *96*(8), pp.1243-1255.

Danesh-Yazdi, M. and Ataie-Ashtiani, B., 2019. Lake Urmia crisis and restoration plan: Planning without appropriate data and model is gambling. *Journal of Hydrology*, *576*, pp.639-651.

DeFlorio, M.J., Waliser, D.E., Guan, B., Ralph, F.M. and Vitart, F., 2019. Global evaluation of atmospheric river subseasonal prediction skill. *Climate Dynamics*, *52*(5), pp.3039-3060.

de Vries, A.J., Tyrlis, E., Edry, D., Krichak, S.O., Steil, B. and Lelieveld, J., 2013. Extreme precipitation events in the Middle East: dynamics of the Active Red Sea Trough. *Journal of Geophysical Research: Atmospheres*, *118*(13), pp.7087-7108.

Dezfuli, A.K., Zaitchik, B.F., Badr, H.S., Evans, J. and Peters-Lidard, C.D., 2017. The role of low-level, terrain-induced jets in rainfall variability in Tigris–Euphrates headwaters. *Journal of hydrometeorology*, *18*(3), pp.819-835.

Dezfuli, A., 2020. Rare atmospheric river caused record floods across the Middle East. *Bulletin of the American Meteorological Society*, *101*(4), pp.E394-E400.

Esfandiari, N. and Lashkari, H., 2020. Identifying atmospheric river events and their paths into Iran. *Theoretical and Applied Climatology*, *140*(3), pp.1125-1137.

Furman, H.K.H., 2003. Dust storms in the Middle East: sources of origin and their temporal characteristics. *Indoor and Built Environment*, *12*(6), pp.419-426.

Gelaro, R., McCarty, W., Suárez, M.J., Todling, R., Molod, A., Takacs, L., Randles, C.A., Darmenov, A., Bosilovich, M.G., Reichle, R. and Wargan, K., 2017. The modern-era retrospective analysis for research and applications, version 2 (MERRA-2). *Journal of climate*, *30*(14), pp.5419-5454.

Gleick, P.H., 2014. Water, drought, climate change, and conflict in Syria. *Weather, Climate, and Society*, *6*(3), pp.331-340.
Guan, B. and Waliser, D.E., 2015. Detection of atmospheric rivers: Evaluation and application of an algorithm for global studies. *Journal of Geophysical Research: Atmospheres*, *120*(24), pp.12514-12535.
Guan, B. and Waliser, D.E., 2019. Tracking atmospheric rivers globally: Spatial distributions and temporal evolution of life cycle characteristics. *Journal of Geophysical Research: Atmospheres*, *124*(23), pp.12523-12552.
Hameed, M., Moradkhani, H., Ahmadalipour, A., Moftakhari, H., Abbaszadeh, P. and Alipour, A., 2019. A review of the 21st century challenges in the food-energy-water security in the Middle East. *Water*, *11*(4), p.682.
Huffman, G.J., Bolvin, D.T., Braithwaite, D., Hsu, K., Joyce, R., Xie, P. and Yoo, S.H., 2015. NASA global precipitation measurement (GPM) integrated multi-satellite retrievals for GPM (IMERG). *Algorithm Theoretical Basis Document (ATBD) Version*, *4*, p.26.
IRNA, 2017. https://www.irna.ir/news/82492773/
Khaniabadi, Y.O., Daryanoosh, S.M., Amrane, A., Polosa, R., Hopke, P.K., Goudarzi, G., Mohammadi, M.J., Sicard, P. and Armin, H., 2017. Impact of Middle Eastern Dust storms on human health. *Atmospheric pollution research*, *8*(4), pp.606-613.
Lavers, D.A. and Villarini, G., 2015. The contribution of atmospheric rivers to precipitation in Europe and the United States. *Journal of Hydrology*, *522*, pp.382-390.
Lelieveld, J., Proestos, Y., Hadjinicolaou, P., Tanarhte, M., Tyrlis, E. and Zittis, G., 2016. Strongly increasing heat extremes in the Middle East and North Africa (MENA) in the 21st century. *Climatic Change*, *137*(1), pp.245-260.
Martin, A., Ralph, F.M., Demirdjian, R., DeHaan, L., Weihs, R., Helly, J., Reynolds, D. and Iacobellis, S., 2018. Evaluation of atmospheric river predictions by the WRF Model using aircraft and regional mesonet observations of orographic precipitation and its forcing. *Journal of Hydrometeorology*, *19*(7), pp.1097-1113.
Masih, I., Uhlenbrook, S., Maskey, S. and Smakhtin, V., 2011. Streamflow trends and climate linkages in the Zagros Mountains, Iran. *Climatic Change*, *104*(2), pp.317-338.
Massoud, E., Massoud, T., Guan, B., Sengupta, A., Espinoza, V., De Luna, M., Raymond, C. and Waliser, D., 2020. Atmospheric Rivers and Precipitation in the Middle East and North Africa (MENA). *Water*, *12*(10), p.2863.
Micklin, P., 2010. The past, present, and future Aral Sea. *Lakes & Reservoirs: Research & Management*, *15*(3), pp.193-213.
Modarres, R., Sarhadi, A. and Burn, D.H., 2016. Changes of extreme drought and flood events in Iran. *Global and Planetary Change*, *144*, pp.67-81.
Molod, A., Takacs, L., Suarez, M. and Bacmeister, J., 2015. Development of the GEOS-5 atmospheric general circulation model: Evolution from MERRA to MERRA2. *Geoscientific Model Development*, *8*(5), pp.1339-1356.
Mundhenk, B.D., Barnes, E.A., Maloney, E.D. and Baggett, C.F., 2018. Skillful empirical subseasonal prediction of landfalling atmospheric river activity using the Madden–Julian oscillation and quasi-biennial oscillation. *NPJ Climate and Atmospheric Science*, *1*(1), pp.1-7.
Nabavi, S.O., Haimberger, L. and Samimi, C., 2016. Climatology of dust distribution over West Asia from homogenized remote sensing data. *Aeolian Research*, *21*, pp.93-107.
Presstv, 2017. Flooding, landslides kill 48 in northwest Iran. Retrieved from https://www.presstv.com/Detail/2017/04/15/518083/Iran-East-Azerbaijan

Ralph, F.M., Neiman, P.J. and Wick, G.A., 2004. Satellite and CALJET aircraft observations of atmospheric rivers over the eastern North Pacific Ocean during the winter of 1997/98. *Monthly Weather Review*, *132*(7), pp.1721-1745.

Ralph, F.M., Neiman, P.J., Wick, G.A., Gutman, S.I., Dettinger, M.D., Cayan, D.R. and White, A.B., 2006. Flooding on California's Russian River: Role of atmospheric rivers. *Geophysical Research Letters*, *33*(13).

Ralph, F.M., Prather, K.A., Cayan, D., Spackman, J.R., DeMott, P., Dettinger, M., Fairall, C., Leung, R., Rosenfeld, D., Rutledge, S. and Waliser, D., 2016. CalWater field studies designed to quantify the roles of atmospheric rivers and aerosols in modulating US West Coast precipitation in a changing climate. *Bulletin of the American Meteorological Society*, *97*(7), pp.1209-1228.

Ralph, F.M., Dettinger, M.D., Cairns, M.M., Galarneau, T.J. and Eylander, J., 2018. Defining "atmospheric river": How the Glossary of Meteorology helped resolve a debate. *Bulletin of the American Meteorological Society*, *99*(4), pp.837-839.

Ralph, F.M., Rutz, J.J., Cordeira, J.M., Dettinger, M., Anderson, M., Reynolds, D., Schick, L.J. and Smallcomb, C., 2019. A scale to characterize the strength and impacts of atmospheric rivers. *Bulletin of the American Meteorological Society*, *100*(2), pp.269-289.

Ramos, A.M., Nieto, R., Tomé, R., Gimeno, L., Trigo, R.M., Liberato, M.L. and Lavers, D.A., 2016. Atmospheric rivers moisture sources from a Lagrangian perspective. *Earth System Dynamics*, *7*(2), pp.371-384.

Razavi, S., Gober, P., Maier, H.R., Brouwer, R. and Wheater, H., 2020. Anthropocene flooding: Challenges for science and society. *Hydrological Processes*, *34*(8), pp.1996-2000.

Raziei, T., Saghafian, B., Paulo, A.A., Pereira, L.S. and Bordi, I., 2009. Spatial patterns and temporal variability of drought in western Iran. *Water Resources Management*, *23*(3), pp.439-455.

Román, M.O., Wang, Z., Sun, Q., Kalb, V., Miller, S.D., Molthan, A., Schultz, L., Bell, J., Stokes, E.C., Pandey, B. and Seto, K.C., 2018. NASA's Black Marble nighttime lights product suite. *Remote Sensing of Environment*, *210*, pp.113-143.

Rougé, C., Tilmant, A., Zaitchik, B., Dezfuli, A. and Salman, M., 2018. Identifying key water resource vulnerabilities in data-scarce transboundary river basins. *Water Resources Research*, *54*(8), pp.5264-5281.

Soleimani, Z., Teymouri, P., Boloorani, A.D., Mesdaghinia, A., Middleton, N. and Griffin, D.W., 2020. An overview of bioaerosol load and health impacts associated with dust storms: A focus on the Middle East. *Atmospheric Environment*, *223*, p.117187.

Tubi, A., Dayan, U. and Lensky, I.M., 2017. Moisture transport by tropical plumes over the Middle East: a 30-year climatology. *Quarterly Journal of the Royal Meteorological Society*, *143*(709), pp.3165-3176.

Voss, K.K., Evan, A.T., Prather, K.A. and Ralph, F.M., 2020. Dusty Atmospheric Rivers: Characteristics and Origins. *Journal of Climate*, *33*(22), pp.9749-9762.

Waliser, D. and Guan, B., 2017. Extreme winds and precipitation during landfall of atmospheric rivers. *Nature Geoscience*, *10*(3), p.179.

Wick, G.A., Neiman, P.J., Ralph, F.M. and Hamill, T.M., 2013. Evaluation of forecasts of the water vapor signature of atmospheric rivers in operational numerical weather prediction models. *Weather and Forecasting*, *28*(6), pp.1337-1352.

Wurtsbaugh, W.A., Miller, C., Null, S.E., DeRose, R.J., Wilcock, P., Hahnenberger, M., Howe, F. and Moore, J., 2017. Decline of the world's saline lakes. *Nature Geoscience*, *10*(11), pp.816-821.

Zereini, F., and H. Hötzl, Eds., 2008. *Climatic Changes and Water Resources in the Middle East and North Africa*. Springer, 552 pp.

Zhang, X., Aguilar, E., Sensoy, S., Melkonyan, H., Tagiyeva, U., Ahmed, N., Kutaladze, N., Rahimzadeh, F., Taghipour, A., Hantosh, T.H. and Albert, P., 2005. Trends in Middle East climate extreme indices from 1950 to 2003. *Journal of Geophysical Research: Atmospheres*, *110*(D22).